$$\underset{\text{athematical}}{M}\overset{\text{odeling}}{\underset{}{\text{MC}}}\overset{\text{omputing}}{}$$

Simulation of heat distribution in the human eye using discontinuous dual reciprocity boundary element method and non-overlapping domain decomposition approach

Ahmedou Bamba S., Ellabib A., El Madkouri A.

Université Cadi Ayyad, Laboratoire de Mathématiques Appliquées et Informatique,
Faculté des Sciences et Techniques,
Avenue Abdelkrim El Khattabi B. P. 549, Marrakesh, Morocco

In this work, a numerical bi-dimensional simulation of heat distribution in the human eye is investigated. A dual reciprocity boundary element method (DRBEM) is applied to obtain the heat distribution in the human eye. The non-overlapping Dirichlet–Neumann domain decomposition method combined with DRBEM is used to find a more accurate representation of heat distribution in the human eye presented for two, three and four subdomains. The result obtained are compared with literature experimental and numerical studies. The simulations of proposed algorithms describe with sufficient accuracy the heat distribution in the human eye.

1. Introduction

The human being is a homeothermic organism, which means that its body temperature is almost constant which is mainly attributed to the existence of the epidermal envelope, the skin. The skin is the first barrier to protect the human body. There is no epidermal envelope to protect the human eye from environmental fluctuations. The human eye is exposed to the temperature of the environment most of the time.

At the end of the 19th century, researchers became interested in the thermal profile of the human eye. At present, the measurement techniques initially used have been abandoned because of their devastating procedures for the human eye. In the early of 1960s, the development of modern technologies, especially the use of infra-red devices, made it possible to obtain measurements of temperature on the surface of the cornea without damaging the human eye. Erfon et al [5] used infra-red techniques and obtained a mean temperature of 34.3°C, while Purslow et al [16] recorded a mean temperature of 35±1.1°C. These infra-red techniques induce measurement errors and present only the measurements of the temperature on the corneal surface without giving any information on the temperature in other components of the eye.

During the last decades, with the availability of high computing power, numerical and mathematical investigations are considered by many researchers as an alternative to experimental techniques. In 1982, Lagendijk [10] using finite difference method (FDM) reported a mean corneal surface temperature of 34.5°C. Later, Scott [18] used a finite element method (FEM) and obtained a temperature of 33.25°C at the surface of the cornea. Ng et al [13] obtained results of the ocular surface temperature using finite element method (FEM) to have a mean of 33.65°C. In 2007, Ooi et al [14] studied the bioheat transfer in the eye using boundary element method (BEM) and reported a mean corneal surface temperature of 33.68°C.

In this paper a discontinuous dual reciprocity boundary element method is adopted for the approximation of heat distribution in the human eye. This work is divided into five sections, in the first one the governing equation of heat distribution in human eye is presented with adequate boundary conditions, next part is devoted to the description of the combination of dual reciprocity method and non overlapping domain decomposition method [2], the forth section give a numerical application of the proposed methods to the investigated problem, finally some conclusions are drawn in the last section.
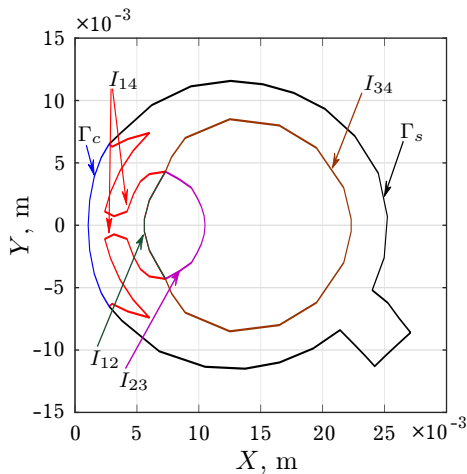
2. The human eye model

Fig. 1. 2D model of the human eye.

We developed a two-dimensional model of the human eye following closely the dimensions in the model in [13]. The human eye is modeled based on anatomical measurements reported in the literature [3,7]. The human eye is divided into four regions the aqueous humor, the lens, the vitreous humor and the sclera. The retina and the choroid are relatively very thin therefore, they are modeled as part of the sclera. The iris and the sclera have the same thermal properties and are modeled together. The cornea is assumed to be part of the aqueous humor since they both have similar thermal properties [4].

The human eye is modeled as comprising four domains, namely the aqueous humor, the lens, the vitreous humor and the sclera which we denote as D_1, D_2, D_3 and D_4, respectively as in Figs. 1 and 2. Thermal properties for each region of the human eye are given in Table 1.
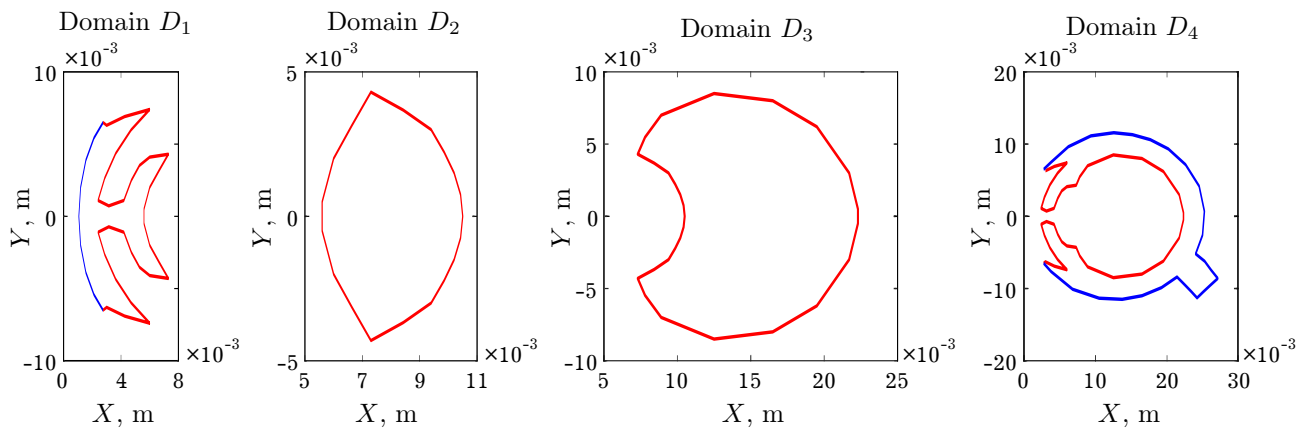

Fig. 2. Four sub-domains of the human eye D_1, D_2, D_3 and D_4.

Table 1. Characteristics of different tissues of the human eye.

Tissue	Thermal conductivity $(\mathrm{W\,m^{-1}K^{-1}})$	Rate of blood perfusion $(\mathrm{s^{-1}})$
Cornea	0.58	0
Aqueous humor	0.58	0
Lens	0.40	0
Iris	1.0042	0
Vitreous humor	0.603	0
Choroid	0.53	0.021
Retina	0.565	0.035
Sclera	1.0042	0

3. Governing equations

3.1. Heat transfer equation

The partial differential equation governing this simulation is the Pennes bioheat equation [15] and its is written as follows

$$\rho\, c_b \frac{\partial T}{\partial t} = \nabla(k_t \nabla T) + \omega_b\, \rho_b\, c_b (T_b - T) + Q + Q_m, \tag{1}$$

where ρ is the density $(\mathrm{kg\,m^{-3}})$, c_b is the specific temperature $(\mathrm{J\,kg^{-1}\,K^{-1}})$, k is the thermal conductivity of local tissue $(\mathrm{W\,m^{-1}\,K^{-1}})$, ω_b is the rate of blood perfusion in the eye $(1/\mathrm{s})$, t is time (s), Q_m is heat generated through metabolism $(\mathrm{W\,m^{-3}})$ and Q is heat generated from external sources such as radiation. Subscript t and b refers to tissue and blood, respectively.

Heat generated by metabolism or by external source is neglected because the human eye is composed mainly of water and we assume that there is no radiations affecting the heat in human eye. For a steady state case, the equation (1) is written

$$\nabla(k_t \nabla T) + \omega_b\, \rho_b\, c_b (T_b - T) = 0. \tag{2}$$

The thermal conductivity of each sub-domain can be found in Table 1.

Moreover, T_b is the blood temperature $37°\mathrm{C}$, C_b is the specific heat of blood $3594\,\mathrm{J/kg°C}$ and ρ_b is the density of blood which are equal to and $1060\,\mathrm{kg/m^3}$.

3.2. Boundary conditions

Boundary conditions are defined on the cornea and the sclera as follow:
— On the sclera Γ_s, the blood flow is acting as a heating source

$$-k\frac{\partial T}{\partial n} = h_{bl}(T - T_{bl}). \tag{3}$$

In the above equation, n is the normal direction to the surface boundary. h_{bl} is the convection coefficient between blood and eye $(65\,\mathrm{W\,m^{-2}K^{-1}})$ and T_{bl} is blood temperature $(37°C)$.
— On the cornea Γ_c, where there are three forms of heat loss through convection, radiation and tears evaporation.

$$-k\frac{\partial T}{\partial n} = h_{amb}(T - T_{amb}) + \sigma\varepsilon(T^4 - T_{amb}^4) + E. \tag{4}$$

In this equation, T_{amb} is the ambient temperature $(25°\mathrm{C})$, h_{amb} is the convection coefficient $(10\,\mathrm{W\,m^{-2}K^{-1}})$ and E is the tear evaporation rate of the eye $(40\,\mathrm{W\,m^{-2}})$. σ is the Stefan Boltzmann constant $(5.67 \times 10^{-8}|,\mathrm{W\,m^{-2}K^{-4}})$ and ε is emissivity 0.975.

4. Approximation methods

In this section, a numerical solution of the problem (2) subject to (3) and (4) is investigated, where a boundary element approach is adopted.

4.1. Discontinuous dual reciprocity boundary element method

In order to develop an integro-differential equation of the considered problem with respect to regions D_i (as illustrated in Fig. 2) a dual reciprocity boundary element method is adopted, i.e.,

$$\lambda(x,y)T_i(x,y) = \int_{\Gamma_i} T_i(s,t)\frac{\partial T^*}{\partial n}(s,t;x,y)\, dS(s,t) - \int_{\Gamma_i} T^*(s,t;x,y)\frac{\partial T_i}{\partial n}(s,t)\, dS(s,t)$$
$$+ \int_{D_i} T^*(s,t;x,y)\left[\frac{w_b\, \rho_b\, c_b}{k_i}(T_b - T_i)\right] dD(s,t) \tag{5}$$

For $(s, t) \in D_i \cup \Gamma_i$ and $i = 1, 2, 3$ and 4. And the jump term is given as:

$$\lambda(s, t) = \begin{cases} 1, & (s, t) \in D_i, \\ 0.5, & (s, t) \in \Gamma_i, \\ 0, & \text{if not.} \end{cases}$$

The fundamental solution $T^*(s, t; x, y)$ is written as follows:

$$T^*(s, t; x, y) = -\frac{1}{2\pi} \log \left(\sqrt{((x - s)^2 + (y - t)^2)} \right)$$

The next step is devoted to the discretization of the boundaries Γ_i into N_i elements, where for each element $\Gamma_i^{(j)}$ two points $(x_i^{(j)}, y_i^{(j)})$ and $(x_i^{(N_i+j)}, y_i^{(N_i+j)})$ are chosen accordingly to the following expressions:

$$\left(x_i^{(j)}, y_i^{(j)} \right) = \left(s_i^{(j)}, t_i^{(j)} \right) + \tau \left(s_i^{(j+1)} - s_i^{(j)}, t_i^{(j+1)} - t_i^{(j)} \right),$$

$$\left(x_i^{(N_i+j)}, y_i^{(N_i+j)} \right) = \left(s_i^{(j)}, t_i^{(j)} \right) + (1 - \tau) \left(s_i^{(j+1)} - s_i^{(j)}, t_i^{(j+1)} - t_i^{(j)} \right),$$

where the two points $\left(s_i^{(j)}, t_i^{(j)} \right)$ and $\left(s_i^{(j+1)}, t_i^{(j+1)} \right)$ denotes the ends points of the element $\Gamma_i^{(j)}$ respectively for $j = 1, 2, \ldots, N_i$, and $\tau \in]0, 0.5[$. We perform a linear approximation of the temperature and the heat flux (denoted $Q_i(s, t)$) in the following form:

$$T_i(s, t) \simeq \left[1 - d_i^{(j)}(s, t) \right] T_i^{(j)} + d_i^{(j)}(s, t) T_i^{(N_i+j)},$$

$$Q_i(s, t) \simeq \left[1 - d_i^{(j)}(s, t) \right] Q_i^{(j)} + d_i^{(j)}(s, t) Q_i^{(N_i+j)}, \tag{6}$$

where

$$d_i^{(j)}(s, t) = \frac{\sqrt{\left(s - s_i^{(j)} \right)^2 + \left(t - t_i^{(j)} \right)^2} - \tau l_i^{(j)}}{(1 - 2\tau) \, l_i^{(j)}}$$

$T_i^{(j)}$ and $T_i^{(N_i+j)}$ denotes the temperature at the points $(x_i^{(j)}, y_i^{(j)})$ and $(x_i^{(N_i+j)}, y_i^{(N_i+j)})$ respectively, and $Q_i^{(j)}$ and $Q_i^{(N_i+j)}$ denotes the heat flux at the points $(x_i^{(j)}, y_i^{(j)})$ and $(x_i^{(N_i+j)}, y_i^{(N_i+j)})$ respectively, $l_i^{(j)}$ is the length of the element $\Gamma_i^{(j)}$.

The task of taking the domain integral in (5) to the boundary is achieved by using a radial basis function approximation of the integrand, in other words we have

$$\left[\frac{w_b \, \rho_b \, c_b}{k_i} (T_b - T_i(s, t)) \right] \simeq \sum_{j=1}^{2N_i+L_i} \alpha^{(j)} R^{(j)}(s, t; s^{(j)}, t^{(j)}), \tag{7}$$

where L_i is the number of internal collocation points in the domain D_i and the radial basis function $R^{(j)}(s, t)$ is given by $R^{(j)}(s, t; s^{(j)}, t^{(j)}) = 1 + \left(\left(s - s^{(j)} \right)^2 + \left(t - t^{(j)} \right)^2 \right) + \left((s - s^{(j)})^2 + (t - t^{(j)})^2 \right)^{3/2}$. The particular solution $\hat{T}$ and the radial basis function are related throw the following relation:

$$\Delta \hat{T} = R.$$

Hence the system (5) can be written as follows

$$\begin{aligned} \lambda(x^{(p)}, y^{(p)}) T_i^{(p)} &= \sum_{k=1}^{N_i} H_{1i}^{(k)}(x^{(p)}, y^{(p)}) T_i^{(k)} + H_{2i}^{(k)}(x^{(p)}, y^{(p)}) T_i^{(N_i+k)} \\ &\quad - G_{1i}^{(k)}(x^{(p)}, y^{(p)}) Q_i^{(k)} - G_{2i}^{(k)}(x^{(p)}, y^{(p)}) Q_i^{(N_i+k)} \\ &= \sum_{j=1}^{2N_i+L_i} \sum_{k=1}^{N_i} H_{1i}^{(k)}(x^{(p)}, y^{(p)}) T_i^{(k)} + H_{2i}^{(k)}(x^{(p)}, y^{(p)}) T_i^{(N_i+k)} \end{aligned}$$

$$- G_{1i}^{(k)}\big(x^{(p)}, y^{(p)}\big) Q_i^{(k)} - G_{2i}^{(k)}\big(x^{(p)}, y^{(p)}\big) Q_i^{(N_i+k)}$$

$$\times \sum_{e=1}^{2N_i+L_i} W_i^{(je)}\left[\frac{w_b\,\rho_b\,c_b}{k_i}(T_b - T_i^{(j)})\right] \tag{8}$$

for $p = 1, 2, \ldots, 2N_i + L_i$ and $i = 1, 2, 3$ and 4. Where $W_i^{(je)}$ are the coefficients of the inverse of the matrix R_i. The system (8) constitutes $2N_i$ unknown (the temperature) and L_i internal unknown $T_i^{(p)}$ for $p = 2N_i + 1, \ldots, 2N_i + L_i$.

The line integrals $H_{1i}^{(k)}$, $H_{2i}^{(k)}$, $G_{1i}^{(k)}$ and $G_{2i}^{(k)}$ are defined by

$$H_{1i}^{(k)}(x, y) = \int_{\Gamma^k} (1 - d_i^{(k)})\frac{\partial T^*}{\partial n}(s, t; x, y)\, dS$$

$$H_{2i}^{(k)}(x, y) = \int_{\Gamma^k} d_i^{(k)}\frac{\partial T^*}{\partial n}(s, t; x, y)\, dS$$

$$G_{1i}^{(k)}(x, y) = \int_{\Gamma^k} (1 - d_i^{(k)})T^*(s, t; x, y)\, dS$$

$$G_{2i}^{(k)}(x, y) = \int_{\Gamma^k} d_i^{(k)}T^*(s, t; x, y)\, dS$$

The non-linearity in (4) is treated using a non-linear modified Newton method with a given precision 10^{-15}.

$$-k\frac{\partial T}{\partial n} = h_{amb}(T - T_{amb}) - \sigma\,\varepsilon\,T_{amb}^4 + E. \tag{9}$$

The given initial approximation is obtained by solving the linear system with using the previous linear boundary condition (8) instead of non-linear condition (4).

4.2. Domain decomposition techniques

In this part a non-overlapping Dirichlet–Neumann domain decomposition method is described, in the first case we decompose the human eye into two sub-domains, then three sub-domains case is investigated, and the last case is devoted to four sub-domains decomposition.

4.2.1. The eye divided into two sub-domains

The first domain decomposition technique is done by decomposing the human eye into two disjoint sub-domains $D_1 \cup D_2$ and $D_3 \cup D_4$ illustrated in Fig. 3. I_{14} and I_{23} are the interfaces between sub-domains D_1 and D_4 and D_2 and D_3, respectively. The Dirichlet–Neumann algorithm used to solve problem (2)–(4) in two sub-domains is given by Algorithm 1.
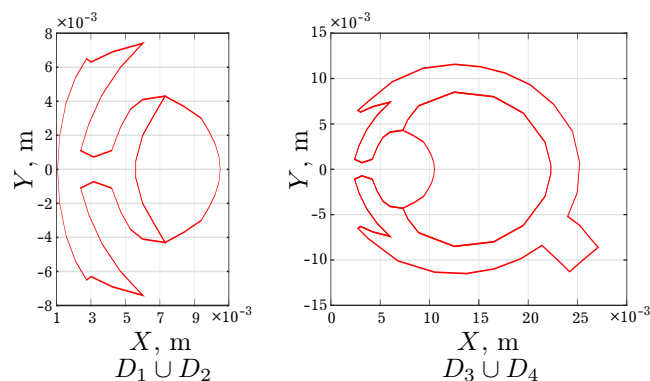
Fig. 3. The decomposition of the human eye into two subdomains. The first subdomain is $D_1 \cup D_2$ composed of the cornea and the lens and the second subdomain $D_3 \cup D_4$ is constitued of the iris, the vitreous humor and the sclera.

Algorithm 1 Two non-overlapping subdomains

Tol, μ_0, $k = 1$, and $error = 1$

While $error \geqslant Tol$

- Solve non-linear problem (10) to obtain $\frac{\partial T_1^k}{\partial n_1}$ on $I_{14} \cup I_{23}$:

$$
\begin{cases}
-\nabla(k_1 \nabla T_1^k) + \omega_b \, \rho_b \, c_b \, T_1^k = \omega_b \, \rho_b \, c_b \, T_b & \text{in} \quad D_1 \cup D_2, \\
-k_1 \frac{\partial T_1^k}{\partial n_1} = h_{amb}(T_1^k - T_{amb}) + \sigma \, \varepsilon\big((T_1^k)^4 - T_{amb}^4\big) + E & \text{on} \quad \Gamma_c, \\
T_1^k = \mu_{k-1} & \text{on} \quad I_{14} \cup I_{23}.
\end{cases}
\tag{10}
$$

- Solve linear problem (11) to obtain T_2^k on $I_{14} \cup I_{23}$:

$$
\begin{cases}
-\nabla(k_2 \nabla T_2^k) + \omega_b \, \rho_b \, c_b \, T_2^k = \omega_b \, \rho_b \, c_b \, T_b & \text{in} \quad D_3 \cup D_4, \\
-k_2 \frac{\partial T_2^k}{\partial n_2} = h_{bl}(T_2^k - T_{bl}) & \text{on} \quad \Gamma_s, \\
-k_2 \frac{\partial T_2^k}{\partial n_2} = k_1 \frac{\partial T_1^k}{\partial n_1} & \text{on} \quad I_{14} \cup I_{23}.
\end{cases}
\tag{11}
$$

- Update:

$$
\mu_k = \mu_{k-1} + \theta\big(T_2^k - \mu_{k-1}\big) \quad \text{on} \quad I_{14} \cup I_{23} \quad \text{and} \quad \theta \in]0, 1[
$$

- Compute:

$$
error = \|\mu_k - \mu_{k-1}\|, \quad k = k + 1.
$$

End while

4.2.2. The eye divided into three sub-domains

The human eye is decomposed into three sub-domains D_1, D_2 and $D_3 \cup D_4$, shown in Fig. 4. I_{12} and I_{14} are the interfaces between sub-domains D_1 and D_2 and D_1 and D_4, respectively. I_{23} refers to the interface between sub-domains D_2 and D_3. The Dirichlet–Neumann algorithm solving problem (2)–(4) is written as in Algorithm 2.
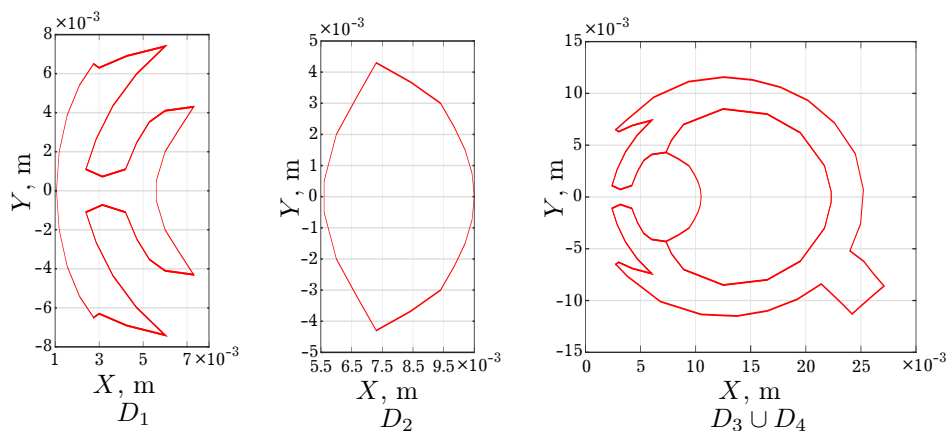
Fig. 4. The decomposition of the human eye into three subdomains. The first subdomain is D_1 composed of the cornea and the aqueous humor, the second subdomain D_2 is the lens and the third subdomain $D_3 \cup D_4$ is constitued of the iris, the vitreous humor and the sclera.

Algorithm 2 Three non-overlapping subdomains

Tol, μ_0^1, μ_0^2, $k = 1$, and $error = 1$

While $error \geqslant Tol$

• Solve non-linear problem (12) to obtain $\frac{\partial T_1^k}{\partial n_1}$ on $I_{14} \cup I_{12}$:

$$
\begin{cases}
-\nabla(k_1 \nabla T_1^k) + \omega_b\,\rho_b\,c_b\,T_1^k = \omega_b\,\rho_b\,c_b\,T_b & \text{in} \quad D_1, \\
-k_1 \frac{\partial T_1^k}{\partial n_1} = h_{amb}\big(T_1 - T_{amb}^k\big) + \sigma\,\varepsilon\big((T_1^k)^4 - T_{amb}^4\big) + E & \text{on} \quad \Gamma_c, \\
T_1^k = \mu_{k-1}^1 & \text{on} \quad I_{14} \cup I_{12}.
\end{cases}
\tag{12}
$$

• Solve linear problem (13) to obtain T_2^k on I_{12} and $\frac{\partial T_2^k}{\partial n_2}$ on I_{23}:

$$
\begin{cases}
-\nabla(k_2 \nabla T_2^k) + \omega_b\,\rho_b\,c_b\,T_2^k = \omega_b\,\rho_b\,c_b\,T_b & \text{in} \quad D_2, \\
-k_2 \frac{\partial T_2^k}{\partial n_2} = k_1 \frac{\partial T_1^k}{\partial n_1} & \text{on} \quad I_{12}, \\
T_2^k = \mu_{k-1}^2 & \text{on} \quad I_{23}.
\end{cases}
\tag{13}
$$

• Solve linear problem (14) to obtain T_3^k on $I_{14} \cup I_{23}$:

$$
\begin{cases}
-\nabla(k_3 \nabla T_3^k) + \omega_b\,\rho_b\,c_b\,T_3^k = \omega_b\,\rho_b\,c_b\,T_b & \text{in} \quad D_3 \cup D_4, \\
-k_3 \frac{\partial T_3^k}{\partial n_3} = h_{bl}\big(T_3^k - T_{bl}\big) & \text{on} \quad \Gamma_s, \\
-k_3 \frac{\partial T_3^k}{\partial n_3} = k_1 \frac{\partial T_1^k}{\partial n_1} & \text{on} \quad I_{14}, \\
-k_3 \frac{\partial T_3^k}{\partial n_3} = k_2 \frac{\partial T_2^k}{\partial n_2} & \text{on} \quad I_{23}.
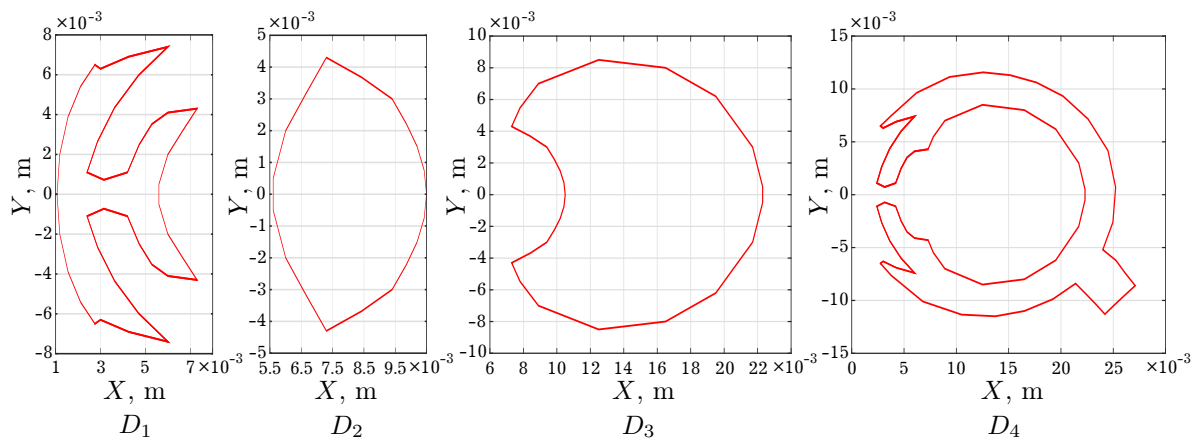\end{cases}
\tag{14}
$$

• Update:

$$
\begin{aligned}
\mu_k^1 &= \mu_{k-1}^1 + \theta_1\big(T_2^k - \mu_{k-1}^1\big) \quad \text{on} \quad I_{12} \quad \text{and} \quad \theta_1 \in\,]0,1[, \\
\mu_k^2 &= \mu_{k-1}^2 + \theta_2\big(T_3^k - \mu_{k-1}^2\big) \quad \text{on} \quad I_{14} \cup I_{23} \quad \text{and} \quad \theta_2 \in\,]0,1[.
\end{aligned}
$$

• Compute:

$$
error = \max\big(\|\mu_k^1 - \mu_{k-1}^1\|, \|\mu_k^2 - \mu_{k-1}^2\|\big) \quad k = k + 1.
$$

End while

4.2.3. The eye divided into four sub-domains

Fig. 5. The decomposition of the human eye into four sub-domains D_1, D_2, D_3 and D_4.

In this part, the human eye is divided into four sub-domains D_1, D_2, D_3 and D_4 presented in Fig. 5. I_{12} and I_{14} are the interfaces between sub-domains D_1 and D_2 and D_1 and D_4. I_{23} refers to the interface between sub-domains D_2 and D_3, while I_{34} is the interface between sub-domains D_3 and D_4. In this case, the Dirichlet–Neumann algorithm solving problem (2)–(4) is written as in Algorithm 3.

Algorithm 3 Four non-overlapping subdomains

Tol, μ_0^1, μ_0^2, μ_0^3, $k = 1$, and $error = 1$

While $error \geqslant Tol$

• Solve non-linear problem (15) to obtain $\frac{\partial T_1^k}{\partial n_1}$ on $I_{14} \cup I_{12}$:

$$\begin{cases} -\nabla(k_1 \nabla T_1^k) + \omega_b \rho_b c_b T_1^k = \omega_b \rho_b c_b T_b & \text{in} \quad D_1, \\ -k_1 \frac{\partial T_1^k}{\partial n_1} = h_{amb}(T_1^k - T_{amb}) + \sigma \varepsilon((T_1^k)^4 - T_{amb}^4) + E & \text{on} \quad \Gamma_c, \\ T_1^k = \mu_{k-1}^1 & \text{on} \quad I_{14} \cup I_{12}. \end{cases} \quad (15)$$

• Solve linear problem (16) to obtain T_2^k on I_{12} and $\frac{\partial T_2^k}{\partial n_2}$ on I_{23}:

$$\begin{cases} -\nabla(k_2 \nabla T_2^k) + \omega_b \rho_b c_b T_2^k = \omega_b \rho_b c_b T_b & \text{in} \quad D_2, \\ -k_2 \frac{\partial T_2^k}{\partial n_2} = k_1 \frac{\partial T_1^k}{\partial n_1} & \text{on} \quad I_{12}, \\ T_2^k = \mu_{k-1}^2 & \text{on} \quad I_{23}. \end{cases} \quad (16)$$

• Solve linear problem (17) to obtain T_3^k on I_{23} and $\frac{\partial T_3^k}{\partial n_3}$ on I_{34}:

$$\begin{cases} -\nabla(k_3 \nabla T_3^k) + \omega_b \rho_b c_b T_3^k = \omega_b \rho_b c_b T_b & \text{in} \quad D_3, \\ -k_3 \frac{\partial T_3^k}{\partial n_3} = k_2 \frac{\partial T_2^k}{\partial n_2} & \text{on} \quad I_{23}, \\ T_3^k = \mu_{k-1}^3 & \text{on} \quad I_{34} \end{cases} \quad (17)$$

• Solve linear problem (18) to obtain T_4^k on $I_{14} \cup I_{34}$:

$$\begin{cases} -\nabla(k_4 \nabla T_4^k) + \omega_b \rho_b c_b T_4^k = \omega_b \rho_b c_b T_b & \text{in} \quad D_4, \\ -k_4 \frac{\partial T_4^k}{\partial n_4} = h_{bl}(T_4^k - T_{bl}) & \text{on} \quad \Gamma_s, \\ -k_4 \frac{\partial T_4^k}{\partial n_4} = k_1 \frac{\partial T_1^k}{\partial n_1} & \text{on} \quad I_{14}, \\ -k_4 \frac{\partial T_4^k}{\partial n_4} = k_3 \frac{\partial T_3^k}{\partial n_3} & \text{on} \quad I_{34}. \end{cases} \quad (18)$$

• Update:

$$\begin{aligned} \mu_k^1 &= \mu_{k-1}^1 + \theta_1(T_2^k - \mu_{k-1}^1) & \text{on} \quad I_{12} & \text{and} \quad \theta_1 \in]0,1[, \\ \mu_k^2 &= \mu_{k-1}^2 + \theta_2(T_3^k - \mu_{k-1}^2) & \text{on} \quad I_{23} & \text{and} \quad \theta_2 \in]0,1[, \\ \mu_k^3 &= \mu_{k-1}^3 + \theta_3(T_4^k - \mu_{k-1}^3) & \text{on} \quad I_{14} \cup I_{34} & \text{and} \quad \theta_3 \in]0,1[. \end{aligned}$$

• Compute:
$$error = \max(\|\mu_k^1 - \mu_{k-1}^1\|, \|\mu_k^2 - \mu_{k-1}^2\|, \|\mu_k^3 - \mu_{k-1}^3\|), \quad k = k + 1.$$

End while

The resolution of all non-linear problems in all algorithms is done using a non-linear modified Newton algorithm.

5. Results and discussion

In this section, to confirm the performance of our method, we performed synthetic tests in which we used application examples where the analytic expression of the solution is known then real experiments have been carried out using data reported in the literature.

5.1. Synthetic tests

In the first set of tests, we used an example of the problem (1)–(4) where the analytical expression of the solution is $T_{ex}(x,y) = \cos(x+y)$, and $k(x,y) = \exp(-x-y)$. We have in Table 2, the errors between approximated solutions T_{num} and analytical solution T_{ex} on the cornea and the sclera, respectively.

Table 2. Error between the analytical solution T_{ex} and the approached solution T_{num} and error between the analytical normal flux Q_{ex} and the approched normal flux Q_{num} on the Cornea and Sclera.

Method	$\|T_{ex} - T_{num}\|_{L^\infty(\Gamma_c)}$		$\|Q_{ex} - Q_{num}\|_{L^\infty(\Gamma_c)}$	
	Cornea	Sclera	Cornea	Sclera
DRBEM	8.18×10^{-6}	8.78×10^{-6}	4.45×10^{-5}	8.78×10^{-6}
Algorithm 1	1.63×10^{-6}	7.39×10^{-7}	2.95×10^{-4}	7.39×10^{-7}
Algorithm 2	6.39×10^{-6}	1.38×10^{-6}	2.81×10^{-5}	1.38×10^{-6}
Algorithm 3	1.16×10^{-6}	2.18×10^{-6}	3.09×10^{-5}	2.18×10^{-6}

### 5.2. Experiments with real data

The main contribution of this work is to present a 2D model of heat distribution in human eye using dual reciprocity boundary element method in conjunction with domain decomposition method. We performed real experiments using parameters reported in Table 1.

5.2.1. Dual reciprocity boundary element method without domain decomposition

The heat distribution on the corneal surface is shown in Fig. 6(left), where the lowest temperature is 33.8188°C and it is located at the center of the cornea, the highest temperature 36.9310°C occurs at the optic nerve where the blood vessels are acting as a heating source. Figure 6(right) plots the temperature variation along papillary axis. Figure 7 presents the heat flux distribution on the corneal surface.
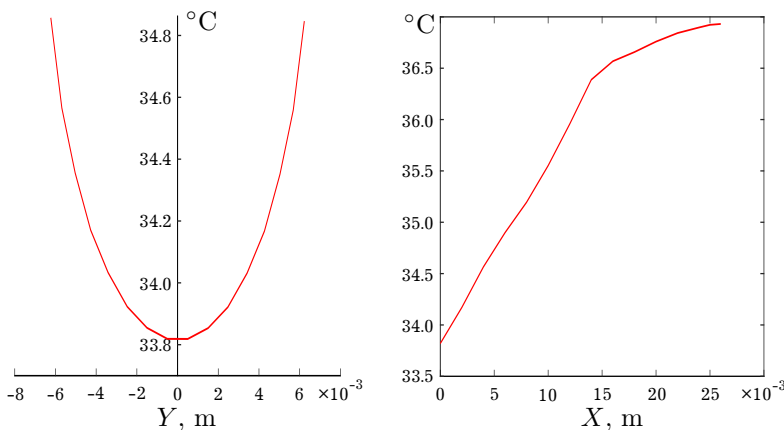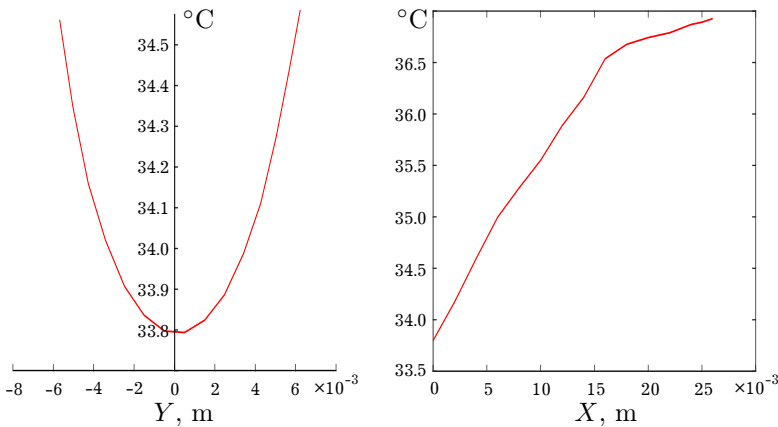

Fig. 6. Temperature ($^\circ$C) on the corneal surface (left) and on the papillary axis (right) obtained by DRBEM without domain decomposition.
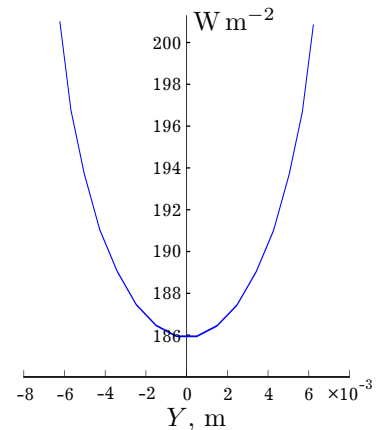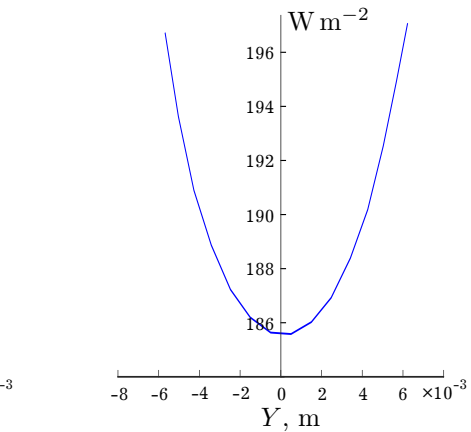
Fig. 7. Normal heat flux on the corneal surface (W m^{-2}) calculated by DRBEM without domain decomposition.

5.2.2. Domain decomposition method: Two sub-domains

In this section, we decomposed the human eye into two disjoint sub-domains $D_1 \cup D_2$ and $D_3 \cup D_4$, we used the Dirichlet–Neumann algorithm to solve (2)–(4). In Fig. 8(left), the lowest temperature $33.7974°C$ is located in the center of the cornea. The temperature increases gradually as one approaches the sclera and the optic nerve as shown in Fig. 8(right). Fig. 9 plots the heat flux on the corneal surface.
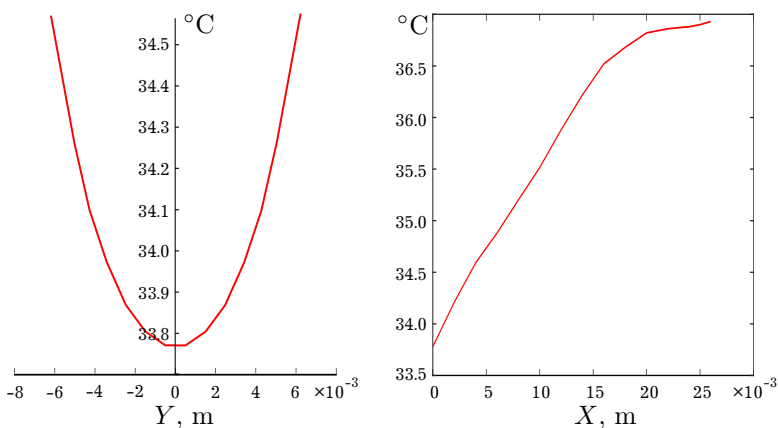

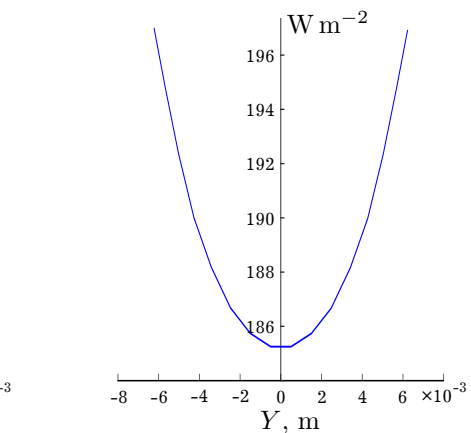**Fig. 8.** Temperature (°C) on the corneal surface (left) and on the papillary axis (right) obtained by Algorithm 1.

Fig. 9. Normal heat flux on the corneal surface (W m^{-2}) calculated byAlgorithm 1.

5.2.3. Domain decomposition method: Three sub-domains

In this part, we partitioned the human eye into three sub-domains D_1, D_2, and $D_3 \cup D_4$, we used the Dirichlet-Neumann algorithm to solve (2)–(4). Fig. 10(left) shows heat distribution on the corneal surface where the lowest temperature, $33.7787°C$, is located at the center of the cornea. The highest temperatures occur at the optic nerve and the sclera. Fig. 10(right) plots the heat variation along papillary axis. Fig. 11 lays out the heat flux distribution on the corneal surface.
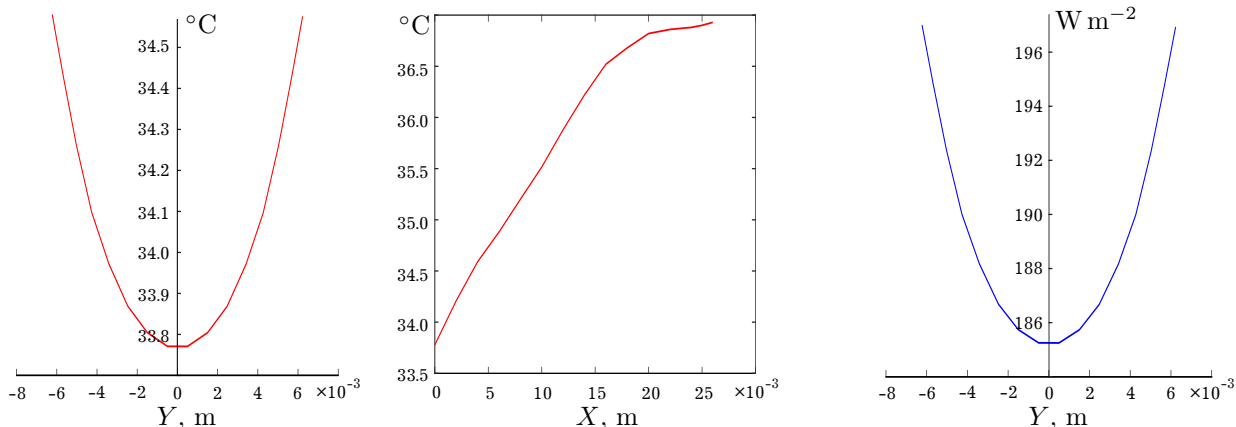

Fig. 10. Temperature (°C) on the corneal surface (left) and on the papillary axis (right) obtained by Algorithm 2.

Fig. 11. Normal heat flux on the corneal surface (W m^{-2}) calculated byAlgorithm 2.

5.2.4. Domain decomposition method: Four sub-domains

In the last numerical simulation, we subdivided the human eye into four sub-domains D_1, D_2, D_3, and D_4. Similarly, we solved problem (2)–(4) using Dirichlet–Neumann algorithm. Fig. 12(left) and Fig. 12(right) show that the numerical value of the temperature at the center of the cornea is $33.7710°C$ and the temperature increases as we go away from the cornea.

Fig. 12. Temperature (°C) on the corneal surface (left) and on the papillary axis (right) obtained by Algorithm 3.

Fig. 13. Normal heat flux on the corneal surface (W m^{-2}) calculated by Algorithm 3.

Table 3. Comparison of values of the temperature at the center of the corneal surface, obtained by the proposed methods and the values obtained by previous numerical and experimental studies.

Method	Temperature (°C)	Reference
DRBEM without DD	33.8188	Present work
Algorithm 1	33.7974	Present work
Algorithm 2	33.7787	Present work
Algorithm 3	33.7710	Present work
Boundary element method	33.65	Ean-Hin Ooi et al [14]
Finite element method	33.68	E. Y. K. Ng et al [13]
Finite element method	33.25	Scott [18]
Finite element method	33.713	Amara [1]
Experimental method: Infra-red	34.80	Mapstone [11]
Experimental method: Infra-red	34.50	Rysa et al [17]
Experimental method: Contact probe	33.67	Horven et al [9]
Experimental method: Infra-red	33.40	Fielder et al [6]
Experimental method: heat flow	34.50	Martin et al [12]

All the methods that have been applied in this study, give values of the temperatures at the center of the cornea between 33.7710°C and 33.8188°C. It is clear from Table 3 that there is a good agreement between our results and past experimental and numerical results. The temperature on the papillary axis is noticed to increase from it lowest value at the center of the corneal surface to a higher temperature at the sclera.

6. Conclusion

In this work, we formulate the dual reciprocity boundary element method to find heat distribution in the 2D model of the human eye. At first, we considered the human eye as one domain, then we applied a non-overlapping Dirichlet–Neumann domain decomposition method by decomposing the human eye into two sub-domains then three sub-domains and in a the last simulation to four sub-domains. Comparing the obtained results with previous numerical and experimental studies our 2D model is an accurate representation of heat distribution in the human eye. The presented model can be used to predict the heat distribution in the case of a tumor in the human eye.

[1] Amara E. H. Numerical investigations on thermal effects of laser ocular media interaction. International Journal of Heat and Mass Transfer. **38** (13), 2479–2488 (1995).

[2] Danumjaya P., Pani A. K. A block monotone domain decomposition algorithm for nonlinear singularly perturbed parabolic problem. International Journal of numerical analysis and modeling. **3** (2), 211–231 (2006).

[3] Charles M. W., Brown N. Dimensions of the human eye relevant to radiation protection (dosimetry). Phys. Med. Biol. **20** (2), 202–218 (1975).

[4] Cicekli U. Computational model for heat transfer in the human eye using the finite element method. M. Sc. Thesis, Department of Civil and Environmental Engineering, Louisiana State University (2003).

[5] Efron N., Young G., Brennan N. A. Ocular surface temperature. Current Eye Research. **8** (9), 901–906 (1989).

[6] Fielder A. R., Winder A. F., Sheridaidah G. A. K., Cooke E. D. Problems with corneal arcus. Transactions of the Ophtalmological Societies of the United Kingdom. **101** (1), 22–26 (1981).

[7] Fontana S. T., Brubaker R. F. Volume and DOF the anterior chamber of the normal aging human eye. Arch. Ophthalmol. **98** (10), 1803–1808 (1980).

[8] Gokul K., Dil Bahadur G., Pushpa R. FEM approach for transient heat transfer in human eye. Appl. Math. **4** (10B), 30–36 (2013).

[9] Horven I., Larsen C. T. Contact probe for corneal temperature measurements. Acta Ophthalmologica. **53** (6), 856–862 (1975).

[10] Lagendijk J. J. A mathematical model to calculate temperature distributions in human and rabbit eyes during hyperthermic treatment. Physics in Medicine and Biology. **27**, 1301–1311 (1982).

[11] Mapstone R. Measurement of corneal temperature. Experimental Eye Research. **7**, 237–243 (1968).

[12] Martin D. K., Fatt I. The presence of a contact lens induces a very small increase in the anterior corneal surface temperature. Acta Ophthalmologica. **64** (5), 512–518 (1986).

[13] Ng E. Y. K., Ooi E. H. FEM simulation of the eye structure with bioheat analysis. Computer Methods and Programs in Biomedicine. **82** (3), 268–276 (2006).

[14] Ooi E. H., Ang W. T., Ng E. Y. K. Bioheat transfer in the human eye: A boundary element approach. Engineering Analysis with Boundary Elements. **31** (6), 494–500 (2007).

[15] Pennes H. H. Analysis of tissue and arterial blood temperatures in the resting foream. J. Appl. Physiol. **1** (2), 93–122 (1948).

[16] Purslow C., Wolffsohn J. S., Santodomingo–Rubido J. The effect of contact lens wear on dynamic ocular surface temperature, Contact Lens and Anterior Eye. Contact Lens & Anterior Eye. The Journal of The British Contact Lens Association. **28** (1), 29–36 (2005).

[17] Rysa P., Sarvaranta J. Thermography of the eye during cold stress. Acta Ophthalmologica. **123**, 234–239 (1973).

[18] Scott J. A. A finite element model of heat transport in the human eye. Physics in Medicine and Biology. **33** (2), 227–241 (1988).

Моделювання розподілу тепла в людському оці за допомогою дуального розривного методу граничних елементів та методу декомпозиції для областей без перекриття

Ахмедоу Бамба С., Еллабиб А., Ел Мадкоури А.

Університет Каді Айяд, Лабораторія прикладної математики та обчислювальної техніки,
Факультет науки і техніки,
Авеню Абделькрим Ель-Хаттабі Б. П. 549, Марракеш, Марокко

У цій роботі досліджено чисельне двовимірне моделювання розподілу тепла в людському оці. Для отримання розподілу тепла в людському оці застосовується дуальний метод граничних елементів (DRBEM). Метод Діріхле–Ноймана для областей без перекриття в поєднанні з DRBEM використовується для пошуку більш точного зображення розподілу тепла в людському оці, яке подається як дві, три та чотири підобласті. Отримані результати порівнюються з літературними експериментальними та чисельними дослідженнями. Моделювання запропонованих алгоритмів з достатньою точністю описує розподіл тепла в людському оці.

Ключові слова: *розподіл тепла, людське око, дуальний метод, метод граничних елементів.*